Mon. Not. R. Astron. Soc. **000**, 1–9 (2004) Printed 2 February 2008 (MN LATEX style file v2.2)

A Realistic Model for Spatial and Mass Distributions of Dark Halo Substructures: An Analytic Approach

Masamune Oguri⋆ and Jounghun Lee†
Department of Physics, School of Science, University of Tokyo, Tokyo 113-0033, Japan

2 February 2008

ABSTRACT
We construct a realistic model for the dark halo substructures, and derive analytically their spatial, mass, and velocity distributions. Basically, our model is a modification of the Press-Schechter theory to account for the dominant dynamical processes that mark the evolution of dark halo substructures such as the tidal stripping and dynamical friction. Our analytic model successfully reproduces all the well known behaviors of the substructure distributions that have been found in recent numerical simulations: the weak dependence of the mass distributions on the host halo mass; the anti-bias of the spatial distribution relative to the dark matter particle components; the nearly power-law shapes of the mass and velocity distributions. We compare our analytic results with recent high-resolution N-body simulation data and find that they are in excellent agreement with each other.

Key words: cosmology: theory — dark matter — galaxies: clusters: general — galaxies: halos — large-scale structure of universe

1 INTRODUCTION

The substructures of dark matter halos have attracted many attentions, especially because of a possible problem they poses in the currently popular cold dark matter (CDM) model. Numerical simulations have confirmed that the CDM model predicts roughly 10% of mass in a dark halo is bound to substructures (Tormen, Diaferio & Syer 1998; Klypin et al. 1999; Okamoto & Habe 1999; Moore et al. 1999; Ghigna et al. 2000; Springel et al. 2001; Zentner & Bullock 2003; De Lucia et al. 2004; Kravtsov, Gnedin & Klypin 2004). Although the current standard CDM paradigm has been very successful in matching the observational data on large scale, it has been noted that the CDM model overpredicts the abundance of substructures compared with that of observed galactic satellites (e.g., Kauffmann, White & Guiderdoni 1993; Moore et al. 1999). This CDM problem on sub-galactic scale is regarded as one of the most fundamental issues that has to be addressed.

It has been proposed that this CDM problem on sub-galactic scale could be resolved by changing radically the nature of dark matter. The proposals include the self-interacting dark matter model (Spergel & Steinhardt 2000), the warm dark matter model (Colín, Avila-Reese & Valenzuela 2000; Bode, Ostriker & Turok 2001), the annihilating dark matter model (Kaplinghat, Knox & Turner 2000), and non-thermally produced dark matter (Lin et al. 2001). Another possibility is to introduce new inflationary models that can produce density fluctuations with small-scale power cut-off such as an inflation model with broken scale-invariance (Kamionkowski & Liddle 2000) and a double hybrid inflation (Yokoyama 2000). However, these rather radical models are gradually in disfavor with recent observations and numerical simulations (e.g., Hennawi & Ostriker 2002; Yoshida et al. 2003).

The problem may be resolved also by taking account of astrophysical processes such as photoionizing background (Somerville 2002) and inefficient star formation in small mass halos (Stoehr et al. 2002). These ideas claim that the observed number of satellite galaxies is small because only very massive substructures contain stars and most substructures are *dark*. To detect these small dark substructures, the gravitational lensing can be a very powerful tool. For instance, we can constrain the amount of substructures through anomalous flux ratios (Mao & Schneider 1998; Metcalf & Madau 2001; Chiba 2002; Dalal & Kochanek 2002), spectroscopy (Moustakas & Metcalf 2003), or monitoring (Yonehara, Umemura & Susa 2003). Although the gravitational lensing allows us to probe the distribution directly, a caveat is the result is dependent on the spatial distribution of substructures (Chen, Kravtsov & Keeton 2003; Evans & Witt 2003). However, these ideas based on the dark substructures may not be consistent with obser-

⋆ E-mail:oguri@utap.phys.s.u-tokyo.ac.jp
† E-mail:lee@utap.phys.s.u-tokyo.ac.jp

vations, either: Recent high-resolution numerical simulations have found that the massive substructures tend to place in the outer part of host halos, which is not the case for the satellites of our Milky way (De Lucia et al. 2004; Taylor, Babul & Silk 2004).

Despite the importance of substructures to understand the structure formation in the universe, most work had to resort to numerical approaches in studying mass and spatial distributions of substructures. Compared with the numerical approach, the analytic approach has an advantage that it allows us to compute distributions in a wide range of parameters, e.g., mass of host halos and power spectrum. This is essential in cosmological applications of substructures, e.g., in computing power spectrum from halo approach (Sheth & Jain 2003; Dolney, Jain & Takada 2004). In contrast, in N-body simulations one needs high force and mass resolutions to overcome "the overmerging" problem (Klypin et al. 1999), which makes the large number of reliable calculations difficult.

There are several attempts to derive the mass function of substructures by using analytic methods (e.g., Fujita et al. 2002; Sheth 2003). These previous approaches, however, were all based on the oversimplified assumptions such as the mass conservation and the uniform spatial distribution of dark halo substructures. They considered only the gravitational merging of substructures, without taking account the effects of other important dynamical processes that drive the substructure evolution, leading to their final distributions. Among them, most important are the mass-loss caused by the global tides of host halos (e.g. Okamoto & Habe 1999), and the orbital decay driven by the dynamical frictions (e.g., Tormen et al. 1998; Kravtsov et al. 2004).

Very recently, Lee (2004), for the first time, developed an analytical formalism for the global substructure mass function by incorporating the effect of tidally driven mass-loss effect and the non-uniform spatial distribution of substructures in dark halos. Yet Lee's approach was still a simplification of reality, using a crude tidal-limit approximation in estimating the tidal mass-loss and also ignoring the effect of dynamical friction which may be more important in estimating the abundance of massive substructures (Hayashi et al. 2003).

In this paper, we construct a more realistic model for the evolution of dark halo substructures than previous approaches by taking account of not only the effect of global tides but also the effect of dynamical friction, and derive analytically the spatial, mass, and velocity distributions of substructures in dark halos. We also compare our analytic results with very recent high-resolution numerical simulations presented by De Lucia et al. (2004).

The plan of our paper is as follows. In §2, we study the effects of global tides and dynamical frictions on the evolution of dark halo substructures, and provide approximation formula to quantify them. Section 3 is devoted to present an analytic formalism for the spatial and mass distributions of substructures. We summarize the results in §4, and we compare our analytic predictions with numerical data in §5. Finally, in §6 we discuss the results and draw final conclusions.

2 GLOBAL TIDES AND DYNAMICAL FRICTIONS

2.1 Tidal Stripping

The most dominant force that drive the dynamical evolution of the dark halo substructures (*subhalos*) are the global tides from host halos (Okamoto & Habe 1999). The global tides from host halos strip the outer parts of subhalos, resulting in the subhalo total disruption or at least significant amount of subhalo mass loss.

For the realistic treatment of the mass-loss caused by the global tides, it is necessary to assign the density profiles to both the host halos and the subhalos. We consider a situation that a subhalo with with virial mass $m_{\rm vir}$ is moving in a circular orbit of radius R from the center of a host halo with virial mass $M_{\rm vir}$. Then we assume that the initial density distributions of both the subhalos and the host halos are well described by the profiles obtained in N-body simulations (Navarro, Frenk & White 1997, hereafter NFW):

$$\rho(R) = \frac{\rho_s}{(R/R_{\rm s})(1+R/R_{\rm s})^2}, \tag{1}$$

where $\rho_{\rm s}$ is the characteristic density that can be computed from the nonlinear overdensity $\Delta_{\rm vir}$, and $R_{\rm s}$ is the halo scale radius. We use the top-hat radius as the virial radius such that

$$R_{\rm vir} = \left(\frac{3M_{\rm vir}}{4\pi\Delta_{\rm vir}\bar{\rho}}\right)^{1/3}, \tag{2}$$

where $\bar{\rho}$ is the mean density of the universe. The ratio of the scale radius $R_{\rm s}$ to the halo virial radius $R_{\rm vir}$ defines the halo concentration parameter C and $M_{\rm vir}$ at redshift z (Klypin et al. 1999):

$$C = \frac{124}{1+z}\left(\frac{M_{\rm vir}}{1h^{-1}M_\odot}\right)^{-0.084}, \tag{3}$$

here we incorporate the redshift dependence found by e.g., Bullock et al. (2001). The halo mass confined within the radius of R can be computed from the following relation:

$$M(R) = M_{\rm vir}\frac{f(X)}{f(C)}, \tag{4}$$

where

$$f(X) \equiv \ln(1+X) - \frac{X}{1+X}, \tag{5}$$

and $X \equiv R/R_{\rm s}$. Equations (1)-(5) are written in terms of the host halo properties but they also hold for the subhalo properties. From here on, the capital letters and the small letters are consistently used for the notation of host halos and subhalos, respectively. For example, M, R, and C represent the mass, the radius, and the concentration parameter of host halos, while m, r, and c are the same quantities for the subhalos.

The effect of global tide can be quantified by the tidal radius, $r_{\rm t}$, that is defined as the radius all the mass of a satellite beyond which gets lost by the global tides. For the realistic case that both the host halos and the subhalos are not point-like masses but have extended profiles as is our case, the tidal radius $r_{\rm t}$ is given as

$$r_{\rm t} = \min(r_{\rm t0}, r_{\rm re}), \tag{6}$$

where $r_{\rm t0}$ and $r_{\rm re}$ are defined as a radius at which gravity equals the tidal force and a radius determined by the resonances, respectively. The following two equations allow us to determine the values of $r_{\rm t0}$ and $r_{\rm re}$:

$$\frac{f(x)}{f(X)} = \left(\frac{x}{X}\right)^3 \left(\frac{r_{\rm s}V_{\rm max}}{R_{\rm s}v_{\rm max}}\right)^2 \left[2 - \frac{X^2}{(1+X)^2 f(X)}\right], \quad (7)$$

$$\frac{f(x)}{f(X)} = \left(\frac{x}{X}\right)^3 \left(\frac{r_{\rm s}V_{\rm max}}{R_{\rm s}v_{\rm max}}\right)^2, \quad (8)$$

where $x \equiv r/r_{\rm s}$ and $X \equiv R/R_{\rm s}$. Here $V_{\rm max}$ and $v_{\rm max}$ represent the maximum circular velocity of the host halo and the subhalo respectively. We approximate that the maximum circular velocity occurs at twice the scale radius (Klypin et al. 1999), $V_{\rm max} = V(2R_{\rm s})$ and $v_{\rm max} = v(2r_{\rm s})$, where the rotation velocities are derived by

$$V^2(R) = \frac{GM_{\rm vir}}{R}\frac{f(X)}{f(C)}, \quad (9)$$

$$v^2(r) = \frac{Gm_{\rm vir}}{r}\frac{f(x)}{f(c)}. \quad (10)$$

Once the tidal radius is determined through the above equations (6)-(10), the final subhalo mass, $m_{\rm f}$, after the tidal stripping effect from the global tides is computed as

$$m_{\rm f} = m_{\rm vir}\frac{f(r_{\rm t}/r_{\rm s})}{f(c)}, \quad (11)$$

for $r_{\rm t} < r_{\rm vir}$ and $m_{\rm f} = m_{\rm vir}$ otherwise.

2.2 Orbital Decay

Since the subhalos reside in very dense environments within the host halos, they undergo dynamical friction. Although the most dominant force that drives the subhalo mass-loss is the global tides from host halos, dynamical friction also plays an important role in driving the subhalo dynamical evolution. It causes the orbital decay of the subhalos, making them more susceptible to strong tidal forces.

The key quantity in describing the orbital decay caused by dynamical friction is the friction time scale $t_{\rm df}$:

$$\frac{dR}{dt} = -\frac{R}{t_{\rm df}}, \quad (12)$$

which can be estimated by the Chandraskekhar's formula:

$$t_{\rm df}(m_{\rm vir}, R) = \frac{1}{2}\left[\frac{\partial \ln M(R)}{\partial \ln R} + 1\right]^{-1} \times \frac{V_{\rm circ}^3(R)}{4\pi G^2 (\ln\Lambda) m_{\rm vir}\rho(R) g(V_{\rm circ}(R)/\sqrt{2}\sigma_r)} \quad (13)$$

where

$$g(\xi) \equiv {\rm erf}(\xi) - \frac{2}{\sqrt{\pi}}\xi e^{-\xi^2}, \quad (14)$$

$$\ln\Lambda = 8, \quad (15)$$

$$\sigma_r^2 = V_{\rm max}^2 \frac{2X(1+X)^2}{f(2)} \int_X^\infty \frac{f(x)}{x^3(1+x)^2} dx. \quad (16)$$

Here we assume that the initial circular velocities of the subhalos follow the Maxwellian distributions (Binney & Tremaine 1987; Klypin et al. 1999), and the Coulomb logarithm Λ has a constant value of 8 since this value is found to give the best result in simulations (Tormen et al. 1998).

Since the dynamical friction timescale is approximately proportional to the radius R (Klypin et al. 1999), the final decayed radius $R_{\rm f}$ of the subhalo during the time interval Δt can be estimated as

$$R_{\rm f} = R_{\rm i}\left(1 - \frac{\Delta t}{t_{\rm df}(m_{vir}, R_{\rm i})}\right), \quad (17)$$

where $R_{\rm i}$ is the initial orbital radius of the subhalo before the orbital decay, and $m_{\rm vir}$ is the initial virial mass of the subhalo before the tidal stripping effect. From here on, we drop the subscript "vir" in denoting the initial virial mass, and use the notation M and $m_{\rm i}$ for representing the virial mass of host halos and the initial virial mass of subhalos, respectively.

The model we adopt in this paper is rather simple, and differs from the ones used in the recent comprehensive studies of these dynamical effects. For instance, Hayashi et al. (2003) showed that the effects of tides may be underestimated in the model described above, and that the impulse approximation results in better agreement with the numerical simulations. Benson et al. (2004) considered the improved dynamical friction model which incorporates noncircular motions and more complicated Coulomb logarithm Λ. Nevertheless we keep this simple model so as to be analytically tractable.

3 DERIVATIONS OF SUBSTRUCTURE DISTRIBUTIONS

In §2, we have investigated the effects of global tides and dynamical frictions on the evolution of the dark matter subhalos, and showed that it is possible under some simplified assumptions to predict the final mass and position of a subhalo from the initial mass and position along with the given host halo mass.

The initial spatial and mass distribution of subhalos can be computed by modifying the popular Press & Schechter (1974, hereafre PS) approach (Lee 2004). Let $n(m_{\rm i}, R_{\rm i}; M, z, z_{\rm i})dR_{\rm i}dm_{\rm i}$ represent the number density of subhalos formed at redshift $z_{\rm i}$ with mass in the range of $[m_{\rm i}, m_{\rm i} + dm_{\rm i}]$ located in a spherical shell of radius $R_{\rm i}$ with thickness of $dR_{\rm i}$ from the center of a host halo with mass M at redshift z. This number density can be written as a product of two distributions:

$$n(m_{\rm i}, R_{\rm i}; M, z, z_{\rm i}) = P(R_{\rm i}; M, z) n(m_{\rm i}|R_{\rm i}; M, z, z_{\rm i}), \quad (18)$$

where $P(R_{\rm i}; M, z)dR_{\rm i}$ is the probability that the subhalo has an orbital radius of $R_{\rm i}$ provided that it is included in a host halo of mass M at redshift z, and $n(m_{\rm i}|R_{\rm i}; M, z, z_{\rm i})dm_{\rm i}$ is the number density of subhalos formed at $z_{\rm i}$ with initial mass in the range of $[m_{\rm i}, m_{\rm i} + dm_{\rm i}]$ provided that it is located at an initial orbital radius of $R_{\rm i}$ from the center of a host halo of mass M at redshift z.

For the probability $P(R_{\rm i}; M, z)$, we make *apriori* assumption that it has a form of the NFW profile, expecting that the subhalos follow initially the distribution of dark matter particles:

$$P(R_{\rm i}; M, z)dR_{\rm i} = \frac{4\pi R_{\rm i}^2 A}{(R_{\rm i}/R_{\rm s})(1 + R_{\rm i}/R_{\rm s})^2} dR_{\rm i}, \quad (19)$$

with

$$A \equiv \frac{1}{4\pi R_{\rm s}^3 f(C)}. \tag{20}$$

Here the amplitude A was determined from the normalization constraint of

$$\int_0^{R_{\rm vir}} P(R_{\rm i}; M, z) dR_{\rm i} = 1. \tag{21}$$

While we normalize the distribution by equation (21), we extend this distribution to $R_{\rm c}$, where the radius upper limit $R_{\rm c}$ represents the effective range of the dynamical friction force beyond which the force is negligible. Since the host halo has an extended density profile (see eq. [1]), the effective range of dynamical friction $R_{\rm c}$ does not necessarily coincide with the virial radius of the host halo. Hence in order to derive the subhalo distribution, we have to consider those subhalos which were initially placed outside the virial radius of the host halo but eventually fell into within the host halo virial radius due to the orbital decay caused by the dynamical friction. We estimate the effective radius of the host halo dynamical friction, to find $R_{\rm c} \approx 100 R_{\rm s}$. Hereafter we use the value of $R_{\rm c} = 10 R_{\rm vir}$ since $R_{\rm vir} \approx 10 R_{\rm s}$. As we will see in §4, however, our results are insensitive to the specific choice of $R_{\rm c}$.

The conditional distribution, $n(m_{\rm i}|R_{\rm i}; M, z, z_{\rm i})$, can be obtained by incorporating the spatial correlation between the subhalo and the host halo into the conditional PS mass function (Yano, Nagashima & Gouda 1996; Lee 2004):

$$n(m_{\rm i}|R_{\rm i}; M, z, z_{\rm i}) dm_{\rm i} = \sqrt{\frac{2}{\pi}} \frac{M}{m_{\rm i}} \left| \frac{\partial \sigma_{\rm s}}{\partial m_{\rm i}} \right| \left| \frac{\partial \beta}{\partial \sigma_{\rm s}} \right| e^{-\beta^2/2} dm_{\rm i}, \tag{22}$$

where

$$\beta \equiv \frac{\delta_{\rm c}(z_{\rm i})}{\sqrt{\sigma_{\rm s}^2 - \sigma_{\rm c}^4/\sigma_{\rm h}^2}} \left(1 - \frac{\delta_{\rm c}(z)}{\delta_{\rm c}(z_{\rm i})} \frac{\sigma_{\rm c}^2}{\sigma_{\rm h}^2} \right), \tag{23}$$

$$\sigma_{\rm s}^2 \equiv \int_{-\infty}^{k(m_{\rm i})} \Delta^2(k) d\ln k, \tag{24}$$

$$\sigma_{\rm h}^2 \equiv \int_{-\infty}^{k(M)} \Delta^2(k) d\ln k, \tag{25}$$

$$\sigma_{\rm c}^2 \equiv \int_{-\infty}^{k(M)} \Delta^2(k) \frac{\sin kR_{\rm i}}{kR_{\rm i}} d\ln k, \tag{26}$$

where $\Delta(k)$ is the dimensionless power spectrum of the linear density field, the wave number $k(M)$ is related to the mass as

$$k(M) = \left(\frac{6\pi^2 \bar{\rho}}{M} \right)^{1/3}, \tag{27}$$

and $\delta_{\rm c}(z)$ is a threshold value of the dimensionless density contrast δ at redshift z given by $\delta_{\rm c}(z) \approx 1.68/D(z)$, where $D(z)$ is the linear growth rate of the density field. For an Einstein De-Sitter universe, it reduces to $\delta_{\rm c}(z) \approx 1.68(1+z)$.

Our use of a NFW profile form for the Lagrangian distribution, $P(R_{\rm i})$ can be justified as follows: The original PS formalism assumes that bound objects form at the local density peaks. Thus, in the strict PS framework, a Gaussian peak profile (Bardeen et al. 1986) has to be used for $P(R_{\rm i})$ to be consistent. However, several numerical simulations (e.g., Katz, Quinn, & Gelb 1993) have found a poor correlation between the location of bound objects and the local density peaks in Lagrangian space. In other words, in spite of the fact that the PS theory happens to be quite successful in estimating the statistically averaged number density of bound objects, it has been shown to fail in predicting the Lagrangian density profiles of bound objects, $P(R_{\rm i})$. All one can say for sure is that no matter what the functional form of $P(R_{\rm i})$ is, when it is mapped to the Eulerian space, it must be close to the NFW profile. Without knowing a correct form of $P(R_{\rm i})$, a possible way to make a best approximation is to use the form of NFW profile itself in Lagrangian space[1]. This guarantees that the corresponding Eulerian profile is NFW, and allows us to use the PS approach in Lagrangian space to the substructure mass function.

The other quantity to be considered is the subhalo formation epoch[2] distribution, dp/dz, since the orbital decay of subhalos depend on the time interval $\Delta t \equiv t - t_{\rm i}$. Lacey & Cole (1993) derived an analytic expression for dp/dz, and Kitayama & Suto (1996) provided a fitting formula to dp/dz, which we adopt here (see Appendix C in Kitayama & Suto 1996).

The analytic steps to reach the final subhalo spatial and mass distributions with taking account of tidal mass-loss and orbital decay caused by dynamical friction are summarized as follows:

(i) We determine the final position $R_{\rm f}$ of a subhalo after the dynamical friction effect through equations (13)-(17).
(ii) We determine the tidal radius $r_{\rm t}$ of the subhalo at the final position $R_{\rm f}$ through equations (6)-(10).
(iii) We abandon those subhalos whose tidal radius $r_{\rm t}$ is larger than its final orbital radius $R_{\rm f}$, assuming that they will get disrupted completely by the tidal stripping effect.
(iv) For the survived subhalos with $r_{\rm t} < R_{\rm f}$, we determine the final mass $m_{\rm f}$ through equation (11).
(v) Finally, we count the cumulative number of those subhalos as function of mass m and radius R.

The above procedures to evaluate the cumulative spatial and mass distributions of the subhalos can be summarized by the following analytical expression:

$$N(>m, >R; M, z) = \int \frac{dp}{dz_{\rm i}} dz_{\rm i} \int_S dm_{\rm i} dR_{\rm i} \times n(m_{\rm i}, R_{\rm i}; M, z, z_{\rm i}). \tag{28}$$

where S represents the following condition:

$$m_{\rm f}(m_{\rm i}, R_{\rm i}, z_{\rm i}) > m, \tag{29}$$

$$R_{\rm f}(m_{\rm i}, R_{\rm i}, z_{\rm i}) > R, \tag{30}$$

$$R_{\rm vir} > R_{\rm f}(m_{\rm i}, R_{\rm i}, z_{\rm i}), \tag{31}$$

$$R_{\rm f}(m_{\rm i}, R_{\rm i}, z_{\rm i}) > r_{\rm t}(m_{\rm i}, R_{\rm i}, z_{\rm i}), \tag{32}$$

In other words, the integration over $dm_{\rm i} dR_{\rm i}$ is performed only those regions in the $m_{\rm i}$-$R_{\rm i}$ plane that satisfy the above

[1] Since we are considering a region which has yet to virialize, it may have a different profile from the NFW profile; for instance, Sheth et al. (2001) considered a time-evolution of such profiles by modifying the scale radius.
[2] The formation epoch is defined as the epoch when a progenitor with a mass of fM is formed. We adopt $f = 1/2$ throughout this paper, which is a standard value used by Lacey & Cole (1993) and in many studies which is a standard choice in this context. We note that our result is rather insensitive to the specific choice of f.

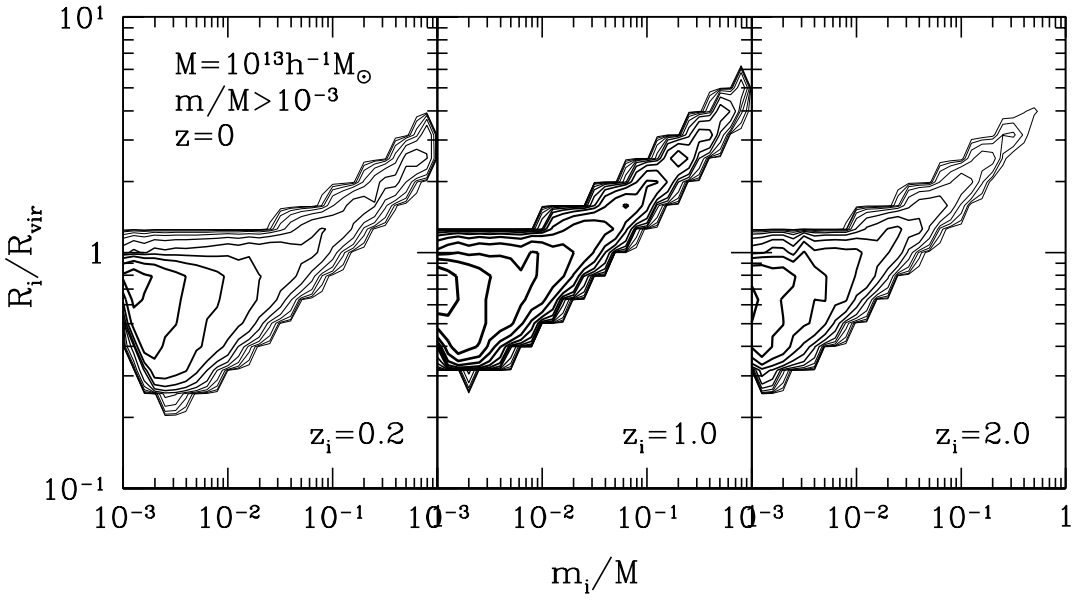

Figure 1. The region of the integral (eq. [28]) in the $m_{\rm i}$-$R_{\rm i}$ plane, for fixed values of $z_{\rm i}$; $z_{\rm i} = 0.2$ (*left*), 1.0 (*middle*), and 2.0 (*right*). We plot contours of the integrand (see eq. [28]) in the logarithmic space; $(dp/dz_{\rm i})n(m_{\rm i}, R_{\rm i}; M, z, z_{\rm i})m_{\rm i}R_{\rm i}$. Darker contours mean larger values, thus darker regions contribute to the integral more.

conditions (eqs. [29]-[32]). To perform an integral with such a complicated boundary condition, it is useful to use a Monte-Carlo integral method.

4 RESULT

As a specific example, we show results of our analytic model in a Lambda dominated CDM model with the choice of the mass density parameter $\Omega_{\rm m} = 0.3$, the vacuum energy density parameter $\Omega_\Lambda = 0.7$, the spectral shape parameter $\Gamma = 0.168$, the dimensionless Hubble constant of $h = 0.7$, and the rms fluctuation normalization $\sigma_8 = 0.9$. We assume the power spectrum of cold dark matter model with primordial spectral index $n_{\rm i} = 1$, and adopt a fitting formula of Bardeen et al. (1986).

In Figure 1, we show the integral region, which is determined by equations (29)-(32), in the $m_{\rm i}$-$R_{\rm i}$ plane for fixed values of $z_{\rm i}$. In reality, we plot contours of the integrand (see eq. [28]) in the logarithmic space. As seen, the region of the integral has a simple topology, and is easily understood; the more massive substructures tend to sink faster, thus they should be in the outer regions of the host halo; when $z_{\rm i}$ is larger the typical value of $R_{\rm i}$ also becomes larger because substructures experience dynamical friction more. However, we also find that the contribution of massive substructures to the integral is rather minor. This is simply because of the small number of massive substructures. Too small $R_{\rm i}$ is not allowed because final sizes of substructures should be smaller than the final distances from the center (eq. [32]). It is also clear from this Figure that our results are insensitive to the value of $R_{\rm c}$ as far as we adopt sufficiently large $R_{\rm c}$, $R_{\rm c} > 5R_{\rm vir}$, since substructures which initially lie very far from the host halo are not counted after all.

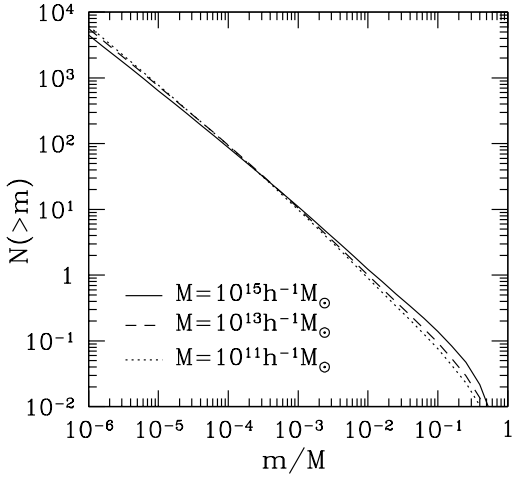

Figure 2. Cumulative mass function of substructures in units of rescaled substructure mass. The redshift is $z = 0$. For the mass of the host halo, we consider $M = 10^{15}h^{-1}M_\odot$ (*solid*), $10^{13}h^{-1}M_\odot$ (*dashed*), and $10^{11}h^{-1}M_\odot$ (*dotted*).

4.1 Mass Distribution

The cumulative mass distribution $N(> m; M, z)$ of subhalos in a given host halo of mass M at redshift z is now straightforwardly obtained by setting $R = 0$ in equation (28):

$$N(> m; M, z) \equiv N(> m, > 0; M, z). \tag{33}$$

Figure 2 plots $N(> m; M, z)$ at redshift $z = 0$ as a function of rescaled subhalo mass for the three different cases of host halo mass M. Note that all the three curves in Figure 2 are very similar to one another, indicating that the subhalo mass distribution is almost independent of the host halo mass. In addition, these curves are close to a power law with

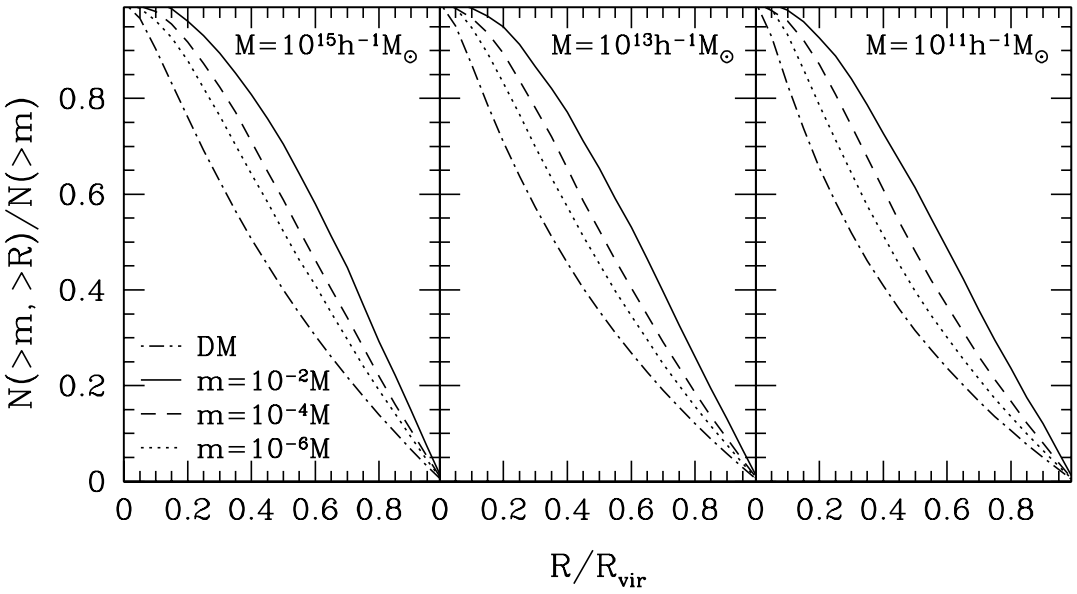

Figure 3. Normalized cumulative spatial distribution of substructures in units of rescaled radius. Mass of the host halo is set to $M = 10^{15}h^{-1}M_\odot$ (*left*), $10^{13}h^{-1}M_\odot$ (*middle*), and $10^{11}h^{-1}M_\odot$ (*right*). We only consider substructures with mass larger than $10^{-2}M$ (*solid*), $10^{-4}M$ (*dashed*), and $10^{-6}M$ (*dotted*). The spatial distribution of smooth dark matter component, which can be calculated from equation (1), is also shown by dash-dotted lines.

the slope of ~ -0.9 in low mass range of $m/M \sim 10^{-5}$ and ~ -1.0 for high mass range of $m/M \sim 10^{-2}$. These findings from our analytic model are all consistent with recent high-resolution numerical simulation results (e.g., Ghigna et al. 2000; De Lucia et al. 2004). It is worth noticing, however, that there is some tendency that the larger the host halos are the slightly more massive subhalos they are assigned to, which is likely because larger host halos form relatively late so that they have relatively little time for their subhalos to undergo orbital decay and lose mass.

4.2 Spatial Distribution

Equation (28) can be interpreted as the cumulative spatial distribution of subhalos for a given mass range. Figure 3 plots the normalized cumulative spatial distribution of subhalos as a function of rescaled radius, and the spatial distributions of the smooth component dark matter for comparison as well. The normalized spatial distribution is defined as $N(>m, >R; M, z)/N(>m; M, z)$. One can see that the spatial distributions of the dark subhalos are *anti-biased* relative to that of the dark matter particle components. This phenomenon has been observed in several numerical simulations (e.g., Ghigna et al. 2000; De Lucia et al. 2004). We also note that more massive subhalos have stronger tendency of anti-bias, which is likely because this anti-bias is caused by tidal stripping and dynamical friction, so that massive subhalos are more affected by those dynamical processes.

4.3 Velocity Distribution

The circular velocity distribution of subhalos is sometimes more useful in practice because it is more readily to be compared with observations (Cole & Kaiser 1989; Shimasaku 1993; Gonzalez et al. 2000; Sheth et al. 2003; Desai et al. 2004). Our analytic model also enables us to compute the circular velocity distribution. Without the tidal stripping effect, the subhalo would retain the original NFW density profile, and thus the subhalo circular velocity would be given by $v_{\rm max} = v(2r_{\rm s})$. However, because of the tidal stripping effect, the subhalos eventually end up with having truncated density profile at truncation radius $\sim 2r_{\rm s}$ (Hayashi et al. 2003). Thus, in our realistic model, the subhalo circular velocity is given as

$$v_{\rm circ} = \begin{cases} v(2r_{\rm s}; m_{\rm i}, z_{\rm i}) & (r_{\rm t} > 2r_{\rm s}), \\ v(r_{\rm t}; m_{\rm i}, z_{\rm i}) & (r_{\rm t} < 2r_{\rm s}). \end{cases} \quad (34)$$

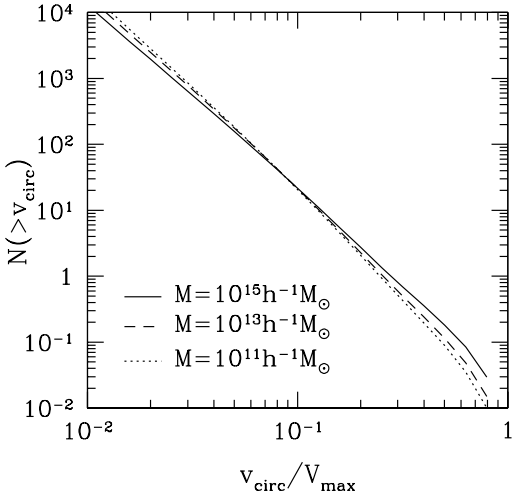

Figure 4. Cumulative circular velocity function of substructures in units of rescaled substructure velocity. For the mass of the host halo, we consider $M = 10^{15}h^{-1}M_\odot$ (*solid*), $10^{13}h^{-1}M_\odot$ (*dashed*), and $10^{11}h^{-1}M_\odot$ (*dotted*).

Thus, the subhalo circular velocity depends not only on the subhalo mass but also on the subhalo position and formation epoch. Using this relation (eq. [34]) along with the subhalo spatial and mass distribution (eq. [28]), we can also evaluate the subhalo velocity distribution.

Figure 4 plots the cumulative circular velocity distribution of subhalos versus the subhalo velocity rescaled by $V_{\rm max}$. Note that the subhalo velocity distribution also shows very weak dependence on the host halo mass, power-law shaped with the slope of ~ -3 around $v_{\rm circ}/V_{\rm max} \sim 10^{-1}$, which is all consistent with numerical detections (Ghigna et al. 2000). And it also has the same tendency as the spatial distribution that the larger a host halo is the more subhalos with high velocity it has.

5 COMPARISON WITH NUMERICAL SIMULATIONS

In this section, we compare our analytic predictions with numerical data from high-resolution simulations performed by De Lucia et al. (2004). In addition to our own analytic model, we also compare the following two models with numerical simulations to demonstrate the importance of dynamical processes that we have included: (i) the model with tidal stripping but without dynamical friction. (ii) the model without tidal stripping and dynamical friction. The models (i) and (ii) basically correspond to those considered in Lee (2004) and Fujita et al. (2002), respectively.

First in Figure 5 we plot our analytic predictions of the subhalo mass distribution with the numerical simulation results (see Fig. 1e of De Lucia et al. 2004). We find that our model agrees quite well with the numerical simulations, while the models without dynamical friction or tidal stripping effect tend to overpredict the number of massive substructures. Those models are inconsistent with the numerical simulations even if we allow them to change their normalization. The success of our model indicates that the effects of tidal stripping and dynamical friction are essential to understand the evolution of subhalos and understand their distributions. For $M = 10^{15}h^{-1}M_\odot$ and $10^{14}h^{-1}M_\odot$, it seems that there is a small difference at $m/M > 0.02$. However, this difference is not significant given the small numbers of host halos (5 and 6, respectively) used for studying the mass distribution in the numerical simulations.

In Figure 6 we compare our analytic predictions on the subhalo spatial distribution with numerical data (see Figure 7 of De Lucia et al. 2004), and show that the two results agree with each other quite well. It is clear from this Figure that our model successfully reproduces the feature found in the numerical simulations that more massive substructures are preferentially located in the outer part of their host halo. This is not the case with the model without dynamical friction. The model without tidal stripping and dynamical friction also shows this feature, because we have assumed also in this model that those subhalos whose radius $r_{\rm vir}$ is larger than its final orbital radius $R_{\rm f}$ will get disrupted completely. However, the distributions themselves are largely inconsistent with the numerical distributions, and rather similar to the distribution of dark matter particles as for smaller substructures. It implies that the dynamical frictions is the main reason for the anti-bias of the subhalo spatial distribution relative to that of the dark matter particles.

6 DISCUSSIONS AND CONCLUSIONS

We have constructed an analytic model for mass and spatial distributions of dark subhalos by taking account of two dominant dynamical processes that drive dominantly subhalo evolution: one is tidal stripping and consequent mass-loss caused by the host halo global tides which remove the outer, and the other is the orbital decay caused by dynamical friction which drives massive subhalos to the inner part of the host halo. We also incorporate the formation epoch variation of the host halo, and the orbital decay of satellite halos outside the host halo virial radius.

We have found that our model predicts nearly power-law mass distribution with weak dependence of host halo mass. The slope of the cumulative mass function turned out to be about -0.9 for low mass substructures $m/M \sim 10^{-5}$, and about -1.0 for larger mass substructures $m/M \sim 10^{-2}$. Next we have predicted the spatial distributions for given mass ranges of substructures. We have found that the spatial distributions are basically anti-biased relative to the smooth component, i.e., the substructures are preferentially located in the outer part of the host halo. The extent of the anti-bias is larger for more massive subhalos. Using our model, we have also predicted the velocity distributions of subhalos. These findings are all consistent with what has been detected by recent high-resolution numerical simulation. So, we have provided physical explanations to those characteristic findings of numerical simulations on the subhalo distributions.

There is some discussion about the accuracy of the Bullock et al. (2001) choice of the evolution of the concentration parameter. For instance, Zhao et al. (2003) found that all high-redshift massive halos have a similar median concentration, $C \sim 3.5$. To see how this affects our results, we repeat the computation by assuming the concentration parameter of equation (3) if $C \geqslant 3.5$, and replace it with $C = 3.5$ if equation (3) yields $C < 3.5$. We find that the substructure mass functions are not changed with this replacement; at $z < 1$ the change is unnoticeable, and even at $z = 2$ it changes the substructure mass function by $< 10\%$.

To test the validity of our model, we have compared our analytic model with the results of the high-resolution numerical simulations by De Lucia et al. (2004). We have showed that mass and spatial distributions of substructures in our model excellently agrees with those in the numerical simulations. For comparison, we have considered the models without tidal stripping or dynamical friction and found that they cannot reproduce the distributions in the numerical simulations. This indicates that the effects of both tidal stripping and dynamical friction are very essential for constructing a realistic model of subhalo distributions.

Yet, it should be noted that we have adopted several simplified assumptions. For instance, we have ignored the effect of encounters between substructures, although it may lead to mass loss comparable to that caused by global tidal stripping (Tormen et al. 1998). We have also assumed spherical halos and circular orbits of subhalos, which are inaccurate because halos in the CDM model are shown to be rather triaxial (Jing & Suto 2002) and the subhalo or-

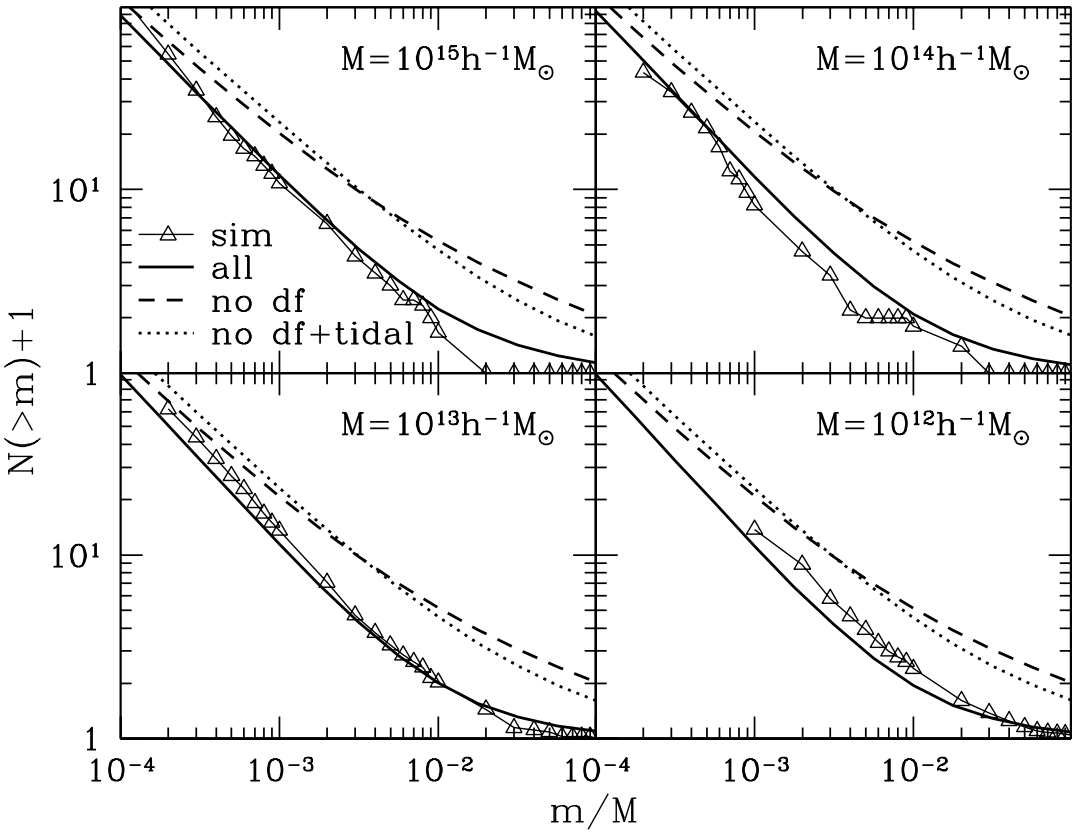

Figure 5. Comparison of the analytic mass distributions (*thick lines*) with numerical ones (*thin lines and triangles*) computed by De Lucia et al. (2004). We consider the host halo mass of $M = 10^{15}h^{-1}M_\odot$ (*upper left*), $10^{14}h^{-1}M_\odot$ (*upper right*), $10^{13}h^{-1}M_\odot$ (*lower left*), and $10^{12}h^{-1}M_\odot$ (*lower right*). As for the analytic mass distributions, we consider not only the fiducial mass distributions in which both dynamical friction and tidal stripping are included (*solid*), but also the mass distributions without dynamical friction (*dashed*) and without dynamical friction and tidal stripping (*dotted*). Here we use $N(m)+1$ rather than $N(>m)$ because in Figure 1e of De Lucia et al. (2004) the host halo itself was included in the cumulative mass function.

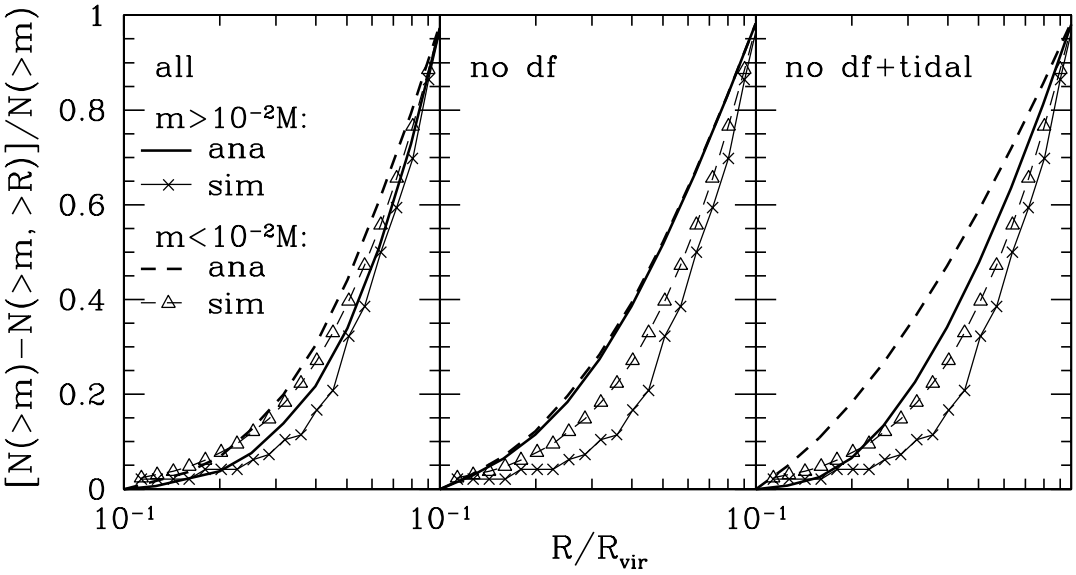

Figure 6. Comparison of the analytic spatial distributions (*thick lines*) with numerical ones (*thin lines and symbols*) computed by De Lucia et al. (2004). Comparison is done for both massive substructures ($m > 10^{-2}M$, denoted by solid lines and/or crosses) and less massive substructures ($10^{-2}M > m > 4\times10^{-4}M$, denoted by dashed lines and/or triangles). From left to right panels, we compare the fiducial analytic model, the model without dynamical friction, and the model without dynamical friction and tidal stripping.

bits are shown to be quite eccentric (Tormen et al. 1998; Hayashi et al. 2003). In spite of these drawbacks of our analytic model, we believe that our model for the subhalo distributions is the most realistic one that has ever been suggested, and that it can be applied to wide fields such as gravitational lensing and halo model of large-scale structure. Our analytic model is quite useful also in calculating the mass and spatial distributions of substructures for different initial conditions such as running primordial power spectrum suggested by the combined analysis of cosmic microwave background and large-scale structure observations (Spergel et al. 2003).

ACKNOWLEDGMENTS

We are very grateful to Gabriella De Lucia for providing numerical simulation data for us, and for many useful suggestions. We also thank an anonymous referee for useful comments and suggestions. M. O. and J. L. acknowledges gratefully the research grant of the JSPS (Japan Society of Promotion of Science) fellowship.

REFERENCES

Bardeen J. M., Bond J. R., Kaiser N., Szalay A. S., 1986, ApJ, 304, 15
Benson A. J., Lacey C. G., Frenk C. S., Baugh C. G., Cole S., 2004, MNRAS, 351, 1215
Binney J., Tremaine S., 1987, Galactic Dynamics (Princeton: Princeton University Press)
Bode P., Ostriker J. P., Turok N., 2001, ApJ, 556, 93
Bullock J. S., Kolatt T. S., Sigad Y., Somerville R. S., Kravtsov A. V., Klypin A. A., Primack J. R., Dekel A., 2001, MNRAS, 321, 559
Chen J., Kravtsov A. V., Keeton C. R., 2003, ApJ, 592, 24
Chiba M., 2002, ApJ, 565, 17
Cole S., Kaiser N., 1989, MNRAS, 237, 1127
Colín P., Avila-Reese V., Valenzuela O., 2000, ApJ, 542, 622
Dalal N., Kochanek C. S., 2002, ApJ, 572, 25
De Lucia G., Kauffmann G., Springel V., White S. D. M., Lanzoni B., Stoehr F., Tormen G., Yoshida N., 2004, MNRAS, 348, 333
Desai V., Dalcanton J. J., Mayer L., Reed D., Quinn T., Governato F., 2004, MNRAS, 351, 265
Dolney D., Jain B., Takada M., 2004, MNRAS, 352, 1019
Evans N. W., Witt H. J., 2003, MNRAS, 345, 1351
Fujita Y., Sarazin C. L., Nagashima M., Yano T., 2002, ApJ, 577, 11
Ghigna S., Moore B., Governato F., Lake G., Quinn T., Stadel J., 2000, ApJ, 544, 616
Gonzalez A. H., Williams K. A., Bullock J. S., Kolatt T. S., Primack J. R., 2000, ApJ, 528, 145
Hayashi E., Navarro J. F., Taylor J. E., Stadel J., Quinn T., 2003, ApJ, 584, 541
Hennawi J. F., Ostriker J. P., 2002, ApJ, 572, 41
Jing Y. P., Suto Y., 2002, ApJ, 574, 538
Kamionkowski M., Liddle A. R., 2000, Phys. Rev. Lett., 84, 4525
Kaplinghat M., Knox L., Turner M. S., 2000, Phys. Rev. Lett., 85, 3335
Katz N., Quinn T., Gelb J. M., 1993, MNRAS, 265, 689
Kauffmann G., White S. D. M., Guiderdoni B., 1993, MNRAS, 264, 201
Kitayama T., Suto Y., 1996, ApJ, 469, 480
Klypin A., Gottlöber S., Kravtsov A. V., Khokhlov A. M., 1999, ApJ, 516, 530
Kravtsov A. V., Gnedin O. Y., Klypin A. A., 2004, ApJ, 609, 482
Lacey C., Cole S., 1993, MNRAS, 262, 627
Lee J., 2004, ApJ, 604, L73
Lin W. B., Huang D. H., Zhang X., & Brandenberger R., 2001, Phys. Rev. Lett., 86, 954
Mao S., Schneider P., 1998, MNRAS, 295, 587
Metcalf R. B., Madau P., 2001, ApJ, 563, 9
Moore B., Ghigna S., Governato F., Lake G., Quinn T., Stadel J., Tozzi P., 1999, ApJ, 524, L19
Moustakas L. A., Metcalf R. B., 2003, MNRAS, 339, 607
Navarro J. F., Frenk C. S., White S. D. M., 1997, ApJ, 490, 493
Okamoto T., Habe A., 1999, ApJ, 516, 591
Press W. H., Schechter P., 1974, ApJ, 187, 425
Sheth, R. K., Diaferio, A., Hui, L., & Scoccimarro, R. 2001, MNRAS, 326, 463
Sheth R. K., 2003, MNRAS, 345, 1200
Sheth R. K., Jain B., 2003, MNRAS, 345, 529
Sheth R. K. et al., 2003, ApJ, 594, 225
Shimasaku K., 1993, ApJ, 413, 59
Stoehr F., White S. D. M., Tormen G., Springel V., 2002, MNRAS, 335, L84
Somerville R. S., 2002, ApJ, 572, L23
Spergel D. N., Steinhardt P. J., 2000, Phys. Rev. Lett., 84, 3760
Spergel D. N. et al., 2003, ApJS, 148, 175
Springel V., White S. D. M., Tormen G., Kauffmann G., 2001, MNRAS, 328, 726
Taylor J. E., Babul A., Silk J., 2004, Satellietes and Tidal Tails (San Francesco:ASP) (astro-ph/0311631)
Tormen G., Diaferio A., Syer D., 1998, MNRAS, 299, 728
Yano T., Nagashima M., Gouda N., 1996, ApJ, 466, 1
Yokoyama J., 2000, Phys. Rev. D, 62, 123509
Yonehara A., Umemura M., Susa H., 2003, PASJ, 55, 1059
Yoshida N., Sokasian A., Hernquist L., Springel V., 2003, ApJ, 591, L1
Zentner A. R., Bullock J. S., 2003, ApJ, 598, 49
Zhao D. H., Jing Y. P., Mo H. J., Börner G., 2003, ApJ, 597, L9